LETTER

https://doi.org/10.1038/s41586-019-1201-8

Superconductivity at 250 K in lanthanum hydride under high pressures

A. P. Drozdov[1,7], P. P. Kong[1,7], V. S. Minkov[1,7], S. P. Besedin[1,7], M. A. Kuzovnikov[1,6,7], S. Mozaffari[2], L. Balicas[2], F. F. Balakirev[3], D. E. Graf[2], V. B. Prakapenka[4], E. Greenberg[4], D. A. Knyazev[1], M. Tkacz[5] & M. I. Eremets[1]*

With the discovery[1] of superconductivity at 203 kelvin in H_3S, attention returned to conventional superconductors with properties that can be described by the Bardeen–Cooper–Schrieffer and the Migdal–Eliashberg theories. Although these theories predict the possibility of room-temperature superconductivity in metals that have certain favourable properties—such as lattice vibrations at high frequencies—they are not sufficient to guide the design or predict the properties of new superconducting materials. First-principles calculations based on density functional theory have enabled such predictions, and have suggested a new family of superconducting hydrides that possess a clathrate-like structure in which the host atom (calcium, yttrium, lanthanum) is at the centre of a cage formed by hydrogen atoms[2–4]. For LaH_{10} and YH_{10}, the onset of superconductivity is predicted to occur at critical temperatures between 240 and 320 kelvin at megabar pressures[3–6]. Here we report superconductivity with a critical temperature of around 250 kelvin within the $Fm\bar{3}m$ structure of LaH_{10} at a pressure of about 170 gigapascals. This is, to our knowledge, the highest critical temperature that has been confirmed so far in a superconducting material. Superconductivity was evidenced by the observation of zero resistance, an isotope effect, and a decrease in critical temperature under an external magnetic field, which suggested an upper critical magnetic field of about 136 tesla at zero temperature. The increase of around 50 kelvin compared with the previous highest critical temperature[1] is an encouraging step towards the goal of achieving room-temperature superconductivity in the near future.

The quest for room-temperature superconductivity is longstanding challenge. Until 1986, superconductivity was considered to be a low-temperature phenomenon, as all known superconducting materials possessed critical temperatures (T_c) below about 30 K. However, the discovery of the cuprate superconductors[7]—copper-based materials with T_c values as high as 164 K (ref. [8]), known as the high-temperature superconductors—initiated extensive research in an attempt to obtain superconductivity at room temperature. However, despite considerable efforts, the maximum value of T_c remained the same for the next 25 years.

The discovery of superconductivity at 203 K in H_3S[1] at high pressures offered another route in the search for high-temperature superconductivity in conventional superconductors[9]. It provided the first confirmation of the predictions of the Bardeen–Cooper–Schrieffer and Migdal–Eliashberg theories regarding the possibility of high-temperature superconductivity in materials with high phonon frequencies[10]. In principle, hydrogen- and carbon-abundant materials can provide the required high frequencies in the phonon spectrum as well as a strong electron–phonon interaction[11,12]. Advances in the experimental search for room-temperature superconductivity came from crystal-structure predictions based on density functional theory[13–16]: the electron and phonon spectra as well as the transition temperatures can be estimated from density functional and Migdal–Eliashberg theories. First-principles theories of superconductivity are also progressing[17,18]. At present, nearly all of the binary hydrides have been studied theoretically[13–15], and calculations are now focusing on the ternary compounds[19].

This broad theoretical search for room-temperature superconductors identified a family of hydride compounds with a clathrate-like structure, and led to studies of CaH_6 (ref. [2]) and subsequently of YH_6 (ref. [20]). In these hydrides, calcium and yttrium are located at the centre of H_{24} cages and act as electron donors contributing to electron pairing, while the hydrogen atoms form weak covalent bonds with each other within the cage. These structures are quite different from that of H_3S, in which each hydrogen atom is connected by a strong covalent bond to the two nearby sulfur atoms. Clathrate-like structures with an even greater hydrogen content, H_{32} cages, were later predicted for YH_{10} and rare-earth hydrides[3] such as LaH_{10} (refs [3,4,21]). These superhydrides can be considered as a close realization of metallic hydrogen and are therefore expected to have high T_c values. Indeed, density functional theory calculations predict T_c values of 235 K at 150 GPa for CaH_6 (ref. [2]), 305–326 K at 250 GPa (ref. [5]) or 303 K at 400 GPa (ref. [3]) for YH_{10}, and approximately 280 K at about 200 GPa for LaH_{10} (refs [3,4]).

The theoretical prediction of materials that show superconductivity near room temperature has motivated experimental verifications; however, such experiments are very challenging. The first lanthanum superhydride was synthesized only recently[22], requiring pressures of greater than 160 GPa and temperatures of around 1,000 K. The X-ray data indicate a stoichiometry of $LaH_{10\pm x}$ ($-1 < x < 2$), which is close to the predicted LaH_{10} (refs [3,5]). In a further experiment, lanthanum was heated with NH_3BH_3 as the hydrogen source under a similar pressure, and the temperature dependence of the resistivity was measured[23]. A decrease in the resistance was observed at around 260 K upon cooling and at around 248 K upon heating the sample, and was assigned to the superconducting transition of $LaH_{10\pm x}$ (ref. [23]). A series of resistance anomalies were also observed at temperatures as high as 275 K. Concurrently, a superconducting transition with $T_c = 215$ K in LaH_x was reported[24]. Neither study provided evidence for a zero-resistance state or any additional confirmation of superconductivity, such as the observation of the Meissner or isotopic effects or the effect of an external magnetic field on the transition temperature.

In the present work we investigated the superconductivity of the lanthanum hydrides. The samples were synthesized directly from lanthanum or LaH_3 and hydrogen under high pressure. A series of lanthanum hydrides with various compositions were produced, as described in Methods and summarized in Supplementary Table 1.

We found a number of superconducting transitions at $T_c \approx 250$ K, 215 K, 110 K and 70 K (Fig. 1, Extended Data Figs. 1–5), at which the electrical resistance decreased sharply to zero. In order to determine the highest value of T_c, we studied its dependence on pressure in LaH_{10}. The data clearly exhibit a 'dome'-like trend: after an initial increase and reaching a maximum value of 250–252 K at around 170 GPa, T_c decreases abruptly at higher pressures (Fig. 1, inset). This is in disagreement with the claim of a continuous increase of T_c up to around 275 K

[1]Max-Planck Institut für Chemie, Mainz, Germany. [2]National High Magnetic Field Laboratory, Florida State University, Tallahassee, FL, USA. [3]NHMFL, Los Alamos National Laboratory, Los Alamos, NM, USA. [4]Center for Advanced Radiation Sources, University of Chicago, Chicago, IL, USA. [5]Institute of Physical Chemistry PAS, Warsaw, Poland. [6]Institute of Solid State Physics RAS, Chernogolovka, Russia. [7]These authors contributed equally: A. P. Drozdov, P. P. Kong, V. S. Minkov, S. P. Besedin, M. A. Kuzovnikov. *e-mail: m.eremets@mpic.de

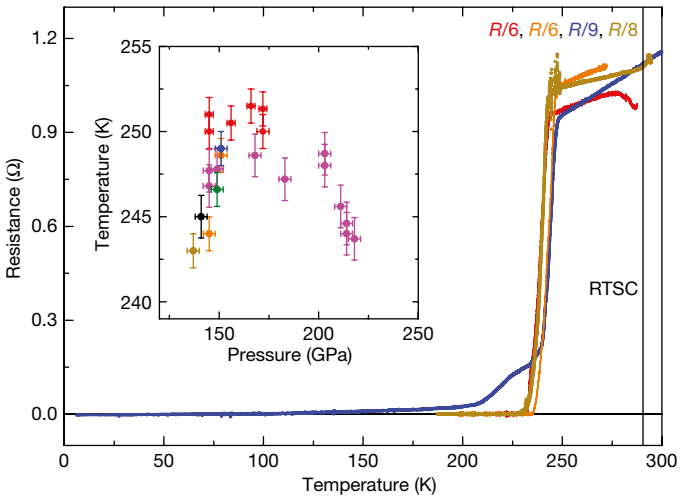

Fig. 1 | The observation of superconductivity in LaH_{10}. Superconducting transitions in the lanthanum superhydride LaH_{10}, measured in different samples synthesized from a La + H_2 mixture. Red curve, sample heated at 145 GPa with $T_c \approx 244$ K, which shifts to around 249 K when the pressure is increased to 151 GPa (orange curve, sample 1); dark yellow curve, sample heated at 135 GPa with $T_c \approx 243$ K (sample 2); blue curve, sample heated at 150 GPa with $T_c \approx 249$ K (sample 3). The red, orange and dark yellow curves show the sharpest transitions to zero resistance upon cooling or heating. The blue curve of sample 3—as is also the case for many other samples—shows an onset of the superconductive transition at around the same temperature, but the sharp transition is distorted by the presence of an impurity phase and/or inhomogeneity in the sample. For clarity, the resistance of the samples was divided by the coefficients shown. The black vertical line at 290 K marks the room-temperature superconductivity (RTSC) limit. The inset shows the dependence of the critical temperature T_c on pressure; the seven different samples are marked in different colours (orange, dark yellow, blue, green, red, magenta and black points correspond to samples 1, 2, 3, 4, 5, 6 and 7, respectively; see Supplementary Table 1). The vertical and horizontal error bars correspond to the uncertainty in the determination of the correct value of T_c (that is, criteria-dependent) and in the precise value of the pressure (inherent error bars of the method used), respectively.

on further increase of pressure to 202 GPa that have been reported previously[23].

To confirm the existence of superconductivity, it is necessary to detect the Meissner effect—that is, the expulsion of magnetic flux from the material. However, magnetization measurements from a diamond anvil cell within a superconducting quantum interference device (SQUID) magnetometer are problematic owing to the small sample volume. The Meissner effect was detected for H_3S (ref. [1]); however, measurements were taken on a sample with a diameter of around 100 μm[1]. Our typical lanthanum hydride samples are much smaller (10–20 μm), such that the strength of their magnetization signal is below the sensitivity of a SQUID magnetometer. Because these small samples also present a challenge for the a.c. magnetic susceptibility method, further experimental developments will be required in order for their magnetization to be fully investigated.

Nevertheless, the superconducting nature of the transition can be verified by its dependence on the external magnetic field. An applied external field reduces T_c in type-II superconductors either through the so-called orbital effect or by breaking the spin-singlet state of the Cooper pair. Figure 2 shows that an applied field of $\mu_0 H = 9$ T indeed reduces the onset of the superconducting transition by about 10 K. The extrapolation of the temperature-dependent upper critical fields $H_{c2}(T)$ towards $T = 0$ K (Fig. 2b) yields values between 95 T and 136 T for $H_{c2}(0)$. Of note is that there are two steps close to 245 K and 230 K in the superconducting transition at zero-field (Fig. 2a, inset). The higher-temperature step gradually broadens with increasing magnetic field and completely disappears above 3 T. This behaviour is consistent with inhomogeneous superconductivity. Although it is difficult to investigate the local inhomogeneity of the superconducting state in a diamond anvil cell, several examples of multi-step transitions in inhomogeneous samples at ambient pressure can be found in the literature[25]. In particular, an anomaly resembling a double transition—as well as resistance peaks at T_c—were also observed in superconducting boron-doped diamond; this anomaly was ascribed to the extinction of individual quasiparticles before the onset of global phase-coherence in strongly inhomogeneous samples[25]. We note that some degree of inhomogeneity is inevitable in samples that are synthesized within the confined space of a diamond anvil cell.

The superconducting phase with $T_c \approx 250$ K at 150 GPa has a face-centred cubic (fcc) lattice structure of space group $Fm\bar{3}m$, in which the refined lattice parameter a is equal to 5.1019(5) Å ($V = 132.80(4)$ Å^3) (Fig. 3b). This fcc structure is in agreement with a previous experimental study (cell volume of 131.9 Å^3 at 172 GPa) and theoretical prediction (128.8 Å^3 at 175 GPa)[22]. Experimentally, the stoichiometry can be estimated from the difference between the cell volumes of the hydride and the initial metal, in which the change is related to the volume occupied by hydrogen atoms. Following this generalization, the extra volume is around 18.2 Å^3 per lanthanum atom (the equation of states for lanthanum was taken from ref. [22]). The volume occupied by one hydrogen atom was accurately determined from the diffraction study of LaH_3 (Extended Data Fig. 1) to be roughly 1.9 Å^3 at 152 GPa. This gives the stoichiometry $LaH_{9.6}$ for the $T_c \approx 250$ K superconductive phase, which is in good agreement with the predicted stoichiometry, LaH_{10} (refs [3,5]).

The change in T_c resulting from the substitution of hydrogen for deuterium provides direct evidence of the superconducting pairing mechanism[9]. To determine the existence of an isotope effect, the T_c of the fcc-LaD_{10} and the fcc-LaH_{10} phases were compared. However, we found that fcc-LaD_{10} is more difficult to prepare than fcc-LaH_{10}, because fcc-LaD_{10} is metastable in the pressure range of 130–160 GPa with respect to a new $P4/nmm$ LaD_{11} phase that is absent in the La-H system. This LaD_{11} phase, with $T_c \approx 140$–168 K (samples 8, 15 and 16 in Supplementary Table 1), has a tetragonally distorted fcc lattice (Fig. 3c), as has been predicted for LaH_{11} in a previous study[3]. In the Methods we also discuss two hexagonal close packed (hcp) phases that frequently occurred in our samples as impurities.

By varying the conditions of the synthesis, we produced the fcc-LaD_{10} phase in two samples (17, 18; Extended Data Figs. 6, 7). In sample 17 the fcc-LaD_{10} phase was found to be mixed with two hexagonal LaD_{10} phases, hcp-I and hcp-II, and an unidentified transparent phase which is clearly an insulating phase. This sample displayed superconductivity with $T_c = 180$ K (Fig. 4). With the aid of subsequent laser heating we identified fcc-LaD_{10} as the phase responsible for the superconductivity. X-ray diffraction showed that heating to around 2,150 K converted fcc-LaD_{10} to the $P4/nmm$ LaD_{11} phase, whereas all other impurity phases remained almost unchanged (Extended Data Fig. 6). These structural changes are in accordance with the changes observed in the temperature-dependency of the resistance; in particular, the onset of superconductivity at 155–160 K corresponds to the T_c of the $P4/nmm$ LaD_{11} phase (Extended Data Figs. 4, 5). Further comparison between the La-H and the La-D systems is presented in Methods.

The isotope coefficient α was determined from the equation $T_c = Am^{-\alpha}$, where m is the isotope mass and A is a constant, assuming $T_c = 249$ K (for fcc-LaH_{10}) and 180 K (for fcc-LaD_{10}) at a pressure of around 150 GPa (Fig. 4). We obtained $\alpha = 0.46$, which is close to the Bardeen–Cooper–Schrieffer value of $\alpha \approx 0.5$ for conventional superconductivity.

In summary, we report the superconductivity of LaH_{10} with a critical temperature of 250 K; to our knowledge, this is the highest critical temperature reported in a superconducting material. We experimentally confirm the prediction of high-temperature superconductivity in superhydrides with a sodalite clathrate-like structure, which was first proposed for CaH_6 (ref. [2]). Our study is a further advance towards room-temperature superconductivity, and also provides evidence that

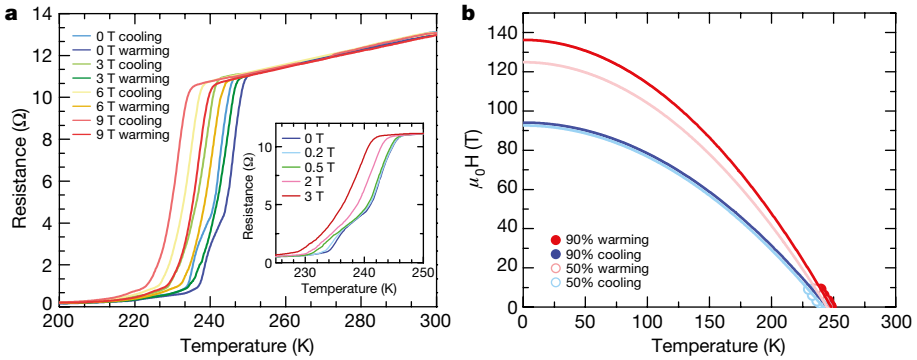

Fig. 2 | Superconducting transition under an external magnetic field. **a**, Electrical resistance as a function of temperature for LaH_{10} (sample 3) under applied magnetic fields of up to 9 T. The width of the superconducting transition remains essentially constant up to 9 T. Both the cooling and the heating temperature sweeps are plotted. The superconducting critical temperatures were determined as the average of the two sweeps. An applied field of 9 T reduces the onset of the superconducting transition from around 250 K (as extracted from the heating curve) to around 240 K. It is notable that the step observed in the superconducting transition measured at zero field, which appears around 245 K, disappears under the application of a modest field of just 3 T (inset); this step probably results from inhomogeneities in the superconducting sample. Similar behaviour was found in disordered superconducting diamond doped with boron[25]. **b**, Upper critical fields as a function of temperature following the criteria of 90% (solid markers) and 50% (open markers) of the resistance in the metallic state, characterized by predominantly linear temperature dependence above T_c. Solid curves are extrapolations resulting from fits to the Ginzburg–Landau expression in order to estimate the upper critical fields at the zero-temperature limit. The temperature dependence of the observed upper critical fields was obtained from the data displayed in Fig. 2a. The upper critical fields near the critical temperature increase nearly linearly with the decrease in temperature. Here, we use a simple Ginzburg–Landau expression $H_{c2}(T) = H_{c2}(0)\left(1-\left(\frac{T}{T_c}\right)^2\right)$ to estimate the upper critical fields $H_{c2}(0)$ in the limit of zero temperature. The Ginzburg–Landau coherence lengths (ξ) deduced from these $H_{c2}(0)$ values range between 1.56 and 1.86 nm.

state-of-the-art methods for the prediction of crystal structures can be very useful in the search for high-temperature superconductors. The current theoretical predictions for room-temperature superconductivity in yttrium superhydrides[3,5,26] motivate further experiments. The observation of superconductivity with very high critical temperatures at high pressures is expected to generate further interest in the search for high-temperature superconductivity at ambient pressure, for example in carbon-based materials[11]. One encouraging example is the discovery of superconductivity at a critical temperature of around 55 K in Q-carbon[27].

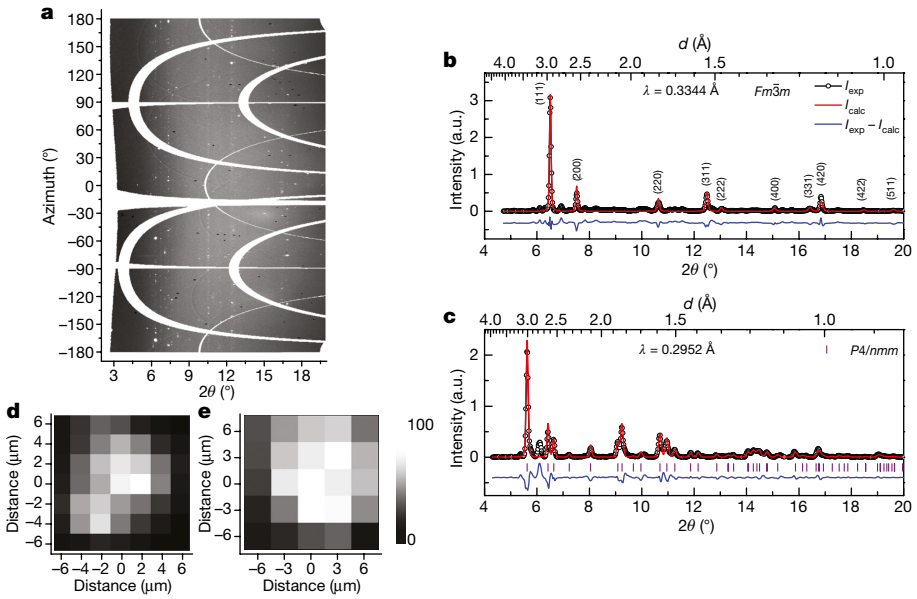

Fig. 3 | Structural analysis. X-ray diffraction studies of superconducting lanthanum hydrides. **a**, Cake representation of the typical X-ray powder diffraction pattern measured for the sample with $T_c \approx 249$ K at 150 GPa (sample 3). The dominant face-centred $Fm\bar{3}m$ phase gives a spotty powder pattern. **b**, **c**, Integrated powder patterns for samples synthesized from the La + H_2 mixture with $T_c \approx 249$ K at 150 GPa (sample 3) (**b**) and the La + D_2 mixture with $T_c \approx 140$ K at 142 GPa (sample 8) (**c**). Indexation and refinement of these powder diffraction patterns yields two different phases: $Fm\bar{3}m$ ($a = 5.1019(5)$ Å, $V = 132.80(4)$ Å^3) and $P4/nmm$ ($a = 3.7258(6)$ Å, $c = 5.0953(12)$ Å, $V = 70.73(2)$ Å^3) with stoichiometries corresponding to $LaH_{9.6}$ and $LaD_{10.6}$, respectively. Both refined crystal structure models are in good agreement with the predicted structures for LaH_{10} (refs [4,5]) and LaH_{11} (ref. [3]), except for the reflection at around 6.10° in **c** that relates to the most intensive 101 reflection of the impurity hcp-I phase. The black, red and blue traces correspond to the experimental data, the fitted data, and the difference between experimental and fitted data, respectively. a.u., arbitrary units. The Le Bail fitting method was chosen to extract the intensities from the powder diffraction pattern, because it is impossible to extract the real intensities of the reflections from the spotty patterns. **d**, **e**, The distribution of the main superconducting LaH_{10} $Fm\bar{3}m$ (**d**) and LaD_{11} $P4/nmm$ (**e**) phases in the samples. The contribution of these phases is estimated using the integral intensity arising from the corresponding phase in the overall powder pattern. These phases comprise more than 80% of the samples, and their distribution throughout the samples is very smooth.

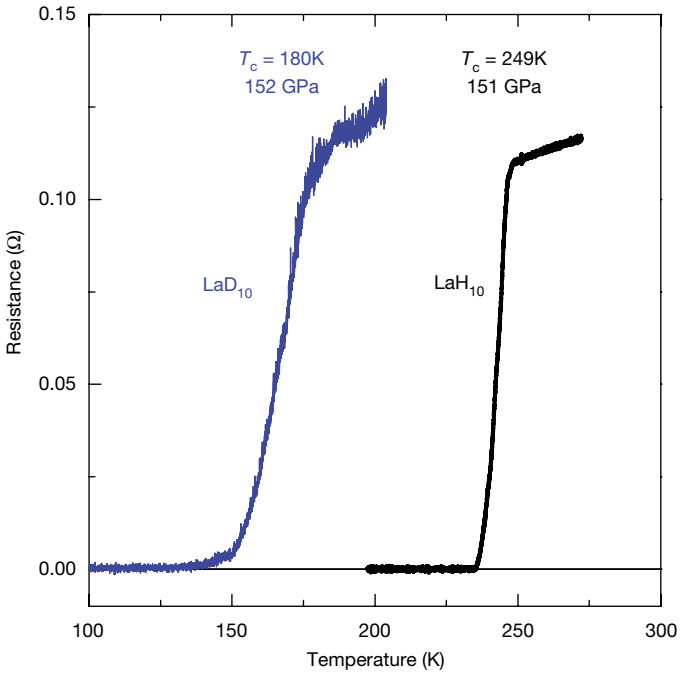

Fig. 4 | The isotope effect. The superconductive transition shifts to markedly lower temperatures after hydrogen is replaced by deuterium in samples with the same fcc crystal structure. The black curve corresponds to LaH_{10} (sample 1) and the blue curve corresponds to LaD_{10} (sample 17).

Online content

Any methods, additional references, Nature Research reporting summaries, source data, statements of data availability and associated accession codes are available at https://doi.org/10.1038/s41586-019-1201-8.

Received: 4 December 2018; Accepted: 4 April 2019;
Published online 22 May 2019.

1. Drozdov, A. P., Eremets, M. I., Troyan, I. A., Ksenofontov, V. & Shylin, S. I. Conventional superconductivity at 203 K at high pressures. *Nature* **525**, 73–76 (2015).
2. Wang, H., Tse, J. S., Tanaka, K., Iitaka, T. i. & Ma, Y. Superconductive sodalite-like clathrate calcium hydride at high pressures. *Proc. Natl Acad. Sci. USA* **109**, 6463–6466 (2012).
3. Peng, F. et al. Hydrogen clathrate structures in rare earth hydrides at high pressures: possible route to room-temperature superconductivity. *Phys. Rev. Lett.* **119**, 107001 (2017).
4. Liu, H. et al. Dynamics and superconductivity in compressed lanthanum superhydride. *Phys. Rev. B* **98**, 100102(R) (2018).
5. Liu, H., Naumov, I. I., Hoffmann, R., Ashcroft, N. W. & Hemley, R. J. Potential high-T_c superconducting lanthanum and yttrium hydrides at high pressure. *Proc. Natl Acad. Sci. USA* **114**, 6990–6995 (2017).
6. Kruglov, I. A. et al. Superconductivity in LaH_{10}: a new twist of the story. Preprint at https://arxiv.org/abs/1810.01113 (2018).
7. Bednorz, J. G. & Mueller, K. A. Possible high T superconductivity in the Ba-La-Cu-O system. *Z. Phys. B* **64**, 189–193 (1986).
8. Schilling, A., Cantoni, M., Guo, J. D. & Ott, H. R. Superconductivity above 130 K in the Hg–Ba–Ca–Cu–O system. *Nature* **363**, 56–58 (1993).
9. Gor'kov, L. P. & Kresin, V. Z. High pressure and road to room temperature superconductivity. *Rev. Mod. Phys.* **90**, 011001 (2018).
10. Allen, P. B. & Dynes, R. C. Transition temperature of strong-coupled superconductors reanalyzed. *Phys. Rev. B* **12**, 905 (1975).
11. Cohen, M. L. Superconductivity in modified semiconductors and the path to higher transition temperatures. *Supercond. Sci. Technol.* **28**, 043001 (2015).
12. Ashcroft, N. W. Hydrogen dominant metallic alloys: high temperature superconductors? *Phys. Rev. Lett.* **92**, 187002 (2004).
13. Pickard, C. J. & Needs, R. J. Ab initio random structure searching. *J. Phys. Condens. Matter* **23**, 053201 (2011).
14. Wang, Y., Lv, J., Zhu, L. & Ma, Y. Crystal structure prediction via particle-swarm optimization. *Phys. Rev. B* **82**, 094116 (2010).
15. Oganov, A. R. & Glass, C. W. Crystal structure prediction using evolutionary algorithms: principles and applications. *J. Chem. Phys.* **124**, 244704 (2006).
16. Zurek, E. in *Handbook of Solid State Chemistry* (eds Dronskowski, R., Kikkawa, S. & Stein, A.) Ch. 15, 571–605 (Wiley-VCH, Weinheim, 2017).
17. Lüders, M. et al. Ab initio theory of superconductivity. I. Density functional formalism and approximate functionals. *Phys. Rev. B* **72**, 024545 (2005).
18. Sanna, A. et al. Ab initio Eliashberg theory: making genuine predictions of superconducting features. *J. Phys. Soc. Jpn.* **87**, 041012 (2018).
19. Boeri, L. in *Handbook of Materials Modeling* (eds Yip, S. & Andreoni, W.) (Springer, Basel, 2018).
20. Li, Y. et al. Pressure-stabilized superconductive yttrium hydrides. *Sci. Rep.* **5**, 9948 (2015).
21. Liu, L. et al. Microscopic mechanism of room-temperature superconductivity in compressed LaH_{10}. *Phys. Rev. B* **99**, 140501(R) (2019).
22. Geballe, Z. M. et al. Synthesis and stability of lanthanum superhydrides. *Angew. Chem. Int. Ed.* **57**, 688 (2018).
23. Somayazulu, M. et al. Evidence for superconductivity above 260 K in lanthanum superhydride at megabar pressures. *Phys. Rev. Lett.* **122**, 027001 (2018).
24. Drozdov, A. P. et al. Superconductivity at 215 K in lanthanum hydride at high pressures. Preprint at https://arxiv.org/abs/1808.07039 (2018).
25. Zhang, G. et al. Bosonic anomalies in boron-doped polycrystalline diamond. *Phys. Rev. Appl.* **6**, 064011 (2016).
26. Heil, C., di Cataldo, S., Bachelet, G. B. & Boeri, L. Superconductivity in sodalite-like yttrium hydride clathrates. Preprint at https://arxiv.org/abs/1901.04001 (2019).
27. Bhaumik, A., Sachan, R., Gupta, S. & Narayan, J. Discovery of high-temperature superconductivity (T_c = 55 K) in B-doped Q-carbon. *ACS Nano* **11**, 11915–11922 (2017).

Acknowledgements M.I.E. thanks the Max Planck Society and the MPI for Chemistry for support, U. Pöschl for encouragement, R. Wittkowski and the staff of the mechanical workshop of the MPI for Chemistry for technical support. We thank S. Sutton for discussion. L.B. is supported by DOE-BES through award DE-SC0002613. S.M. acknowledges support from the FSU Provost Postdoctoral Fellowship Program. The National High Magnetic Field Laboratory acknowledges support from the US NSF Cooperative Grant number DMR-1644779 and the state of Florida. Portions of this work were performed at GeoSoilEnviro CARS (The University of Chicago, Sector 13), Advanced Photon Source (APS), Argonne National Laboratory. GeoSoilEnviro CARS is supported by the National Science Foundation – Earth Sciences (EAR – 1634415) and Department of Energy – GeoSciences (DE-FG02-94ER14466). This research used resources of the Advanced Photon Source, a US Department of Energy (DOE) Office of Science User Facility operated for the DOE Office of Science by Argonne National Laboratory under contract number DE-AC02-06CH11357.

Reviewer information *Nature* thanks James J. Hamlin and the other anonymous reviewer(s) for their contribution to the peer review of this work.

Author contributions A.P.D., P.P.K., V.S.M., S.P.B., M.A.K., M.T. and D.A.K. prepared the samples and measured the superconducting transition. S.M., F.F.B., L.B. and D.E.G. performed studies under external magnetic fields. V.B.P., E.G., V.S.M. and M.A.K. performed X-ray diffraction studies. M.I.E., V.S.M. and S.M. wrote the manuscript, with input from all co-authors. M.I.E. guided the work.

Competing interests The authors declare no competing interests.

Additional information
Extended data is available for this paper at https://doi.org/10.1038/s41586-019-1201-8.
Supplementary information is available for this paper at https://doi.org/10.1038/s41586-019-1201-8.
Reprints and permissions information is available at http://www.nature.com/reprints.
Correspondence and requests for materials should be addressed to M.I.E.
Publisher's note: Springer Nature remains neutral with regard to jurisdictional claims in published maps and institutional affiliations.

METHODS

We typically synthesized lanthanum hydride via a direct reaction of lanthanum (Alfa Aesar 99.9%) and hydrogen (99.999%) at high pressures. A piece of La was placed into a hole that was drilled in an insulating gasket. Sample handling and initial loading of the anvils were done in an inert N_2 atmosphere in a glove box with residual contents of O_2 and H_2O of <0.1 p.p.m., so the sample was isolated from the surrounding atmosphere. Then the diamond anvil cell (DAC) was transferred into the gas loader, where the anvils were taken apart under a hydrogen atmosphere. The hydrogen gas was then pressurized up to about 0.1 GPa, and the DAC was clamped; the pressure was typically increased to around 2 GPa during the clamping. After that, the DAC was extracted from the gas loader, and the pressure was further increased to a desirable value of 120–190 GPa.

Heating of the sample with a laser leads to the formation of various hydrides (Extended Data Figs. 1–5). The formation of a particular hydride depends on the pressure, heating temperature, and the amount of hydrogen surrounding the sample. Hydrides containing a large amount of hydrogen (superhydrides) (Extended Data Figs. 3–5) were synthesized only under an evident excess of hydrogen. Under a hydrogen-deficient environment, LaH_3 (Extended Data Fig. 1) or various different phases can form (Extended Data Figs. 1, 2, 5).

For the thermal treatment, one-sided pulsed radiation from a YAG laser was focused onto a spot with a diameter of ~10 μm. The sample can be heated up to ~1,500 K, but typically the temperature remained below ~700 K as we did not observe glowing. This gentle heating was sufficient to initiate the reaction as the sample expanded and reflected light from the spot on which the laser was focused. The laser spot was scanned over the sample to ensure that the chemical reaction was as complete and uniform as possible. Some samples were prepared not from elemental lanthanum as a starting material but from LaH_3, which was prepared and analysed according to a previous method[28]. One of the advantages of this method is that the initial hydrogen content is higher. Finally, we found that the superhydride with $T_c = 250$ K could be synthesized even without laser heating; it was formed just by maintaining a clamped mixture of LaH_3 and hydrogen under high pressure (~140 GPa) at room temperature for about two weeks (sample 7).

To determine the isotopic effect, we substituted the ^{1}H isotope of hydrogen by ^{2}H (deuterium; 99.75% purity).

The necessity of performing electrical measurements to obtain a direct proof of superconductivity brings other complications. Typically, the diamonds used in DACs had a culet with a diameter of 40–50 μm and were bevelled at 8° to a diameter of about 250 μm. Tantalum electrodes were sputtered onto the surface of one of the diamond anvils in the van der Pauw four-probe geometry. The total resistance of the current leads was typically about 100 Ω per electrode. A four-probe measurement scheme was essential to separate the sample signal from the parasitic resistance of the current leads. A metallic gasket (T301 steel) was electrically separated from the electrodes by an insulating layer. We prepared this layer from a mixture of epoxy and CaF_2 (or a number of other similar materials, for example, MgO, $CaSO_4$, cubic boron nitride, Al_2O_3). The most difficult aspect is to ensure electrical contact between the sample and the electrodes. To achieve this, the sample should be large enough to be squeezed between the anvils and pressed against the electrodes, but also small enough to accommodate an excess of surrounding hydrogen. Typical sizes for these samples were 5–10 μm. The laser heating of the pressurized samples is another experimental challenge owing to the high thermal conductivity and comparatively high volume of the diamond anvils.

After the synthesis, the temperature dependence of the electrical resistance was measured upon cooling and heating of the samples. Hysteresis was observed during this cycling owing to the thermal mass of the pressure cell. We present resistance measurements upon heating the DAC as it yields a more accurate temperature reading: the cell was heated slowly (~0.2 K min^{-1}) under an isothermal environment (no coolant flow). The temperature was measured by a Si diode thermometer attached to the DAC with an accuracy of about 0.1 K. All electrical measurements were performed at a current in the range of 10^{-5} to 10^{-3} A; the value of the current showed no apparent effect on the T_c.

The pressure was measured from the frequency of the vibron of the hydrogen surrounding the sample[29], and from the edge of the Raman signal from diamond pressure scale[30]. Typically, the pressure values determined from the H_2 (D_2) vibron were lower than the values determined from the diamond Raman edge scale by 10–30 GPa at pressures of about 150 GPa. We used the hydrogen (deuterium) scale throughout the manuscript (except for a few cases in which the hydrogen vibron could not be observed). This scale is better in comparison with the diamond scale, which is based on the stresses in diamond adjusting the cavity containing the sample and hydrogen. Hydrogen is very soft even in the solid state and smoothly presses the sample. It is a hydrostatic medium and thus the pressure is uniform over the hydrogen in the cavity. Therefore, the peak of the hydrogen vibron is sharp and its energy can be measured accurately, and the corresponding pressures can be determined with accuracy greater than ±3 GPa. The pressure inside the sample is close to the hydrogen pressure; even the lanthanum hydride sample is squeezed between the anvils. This follows from scanning of the sample—the pressure is the same when measured over the sample or over the hydrogen. The pressure at scanning was measured with the aid of the diamond edge scale—this method is sensitive to changes in local pressures with spatial resolution of few micrometres. The close pressure values for hydrogen and the sample are to be expected for an apparently soft hydride sample.

The T_c was determined from the onset of superconductivity: the point of apparent deviation in the temperature dependence of resistance from the normal metallic behaviour (Extended Data Fig. 2).

Altogether, we found obvious superconductive transitions in 19 samples of lanthanum hydrides, including in eight samples of deuterium counterparts (Supplementary Table 1). The rate of successful experiments (the sample was loaded with hydrogen, laser heated, and four electrodes contacted the sample) was about 20%. Superconductivity was found in the majority of cases. In approximately half of the cases the sample was surrounded by a large amount of H_2 (or D_2). X-ray diffraction was measured for six hydride samples and eight deuteride samples (Supplementary Table 1).

We used three types of DAC. DACs with diameters of 20 mm and 8.8 mm were made of non-magnetic materials, suitable for measurements under magnetic fields using a 9 T Quantum Design Physical Property Measurement System (PPMS). The X-ray diffraction measurements were performed at wavelengths of 0.3344 Å and 0.2952 Å, X-ray spot size of around 3 × 4 μm, and Pilatus 1M CdTe detector at the beamline 13-IDD at GSECARS, Advanced Photon Source, Argonne National Laboratory. Primary processing and integration of the powder patterns were carried out using the Dioptas software[31]. The Indexing and refinement were performed with the GSAS and EXPGUI packages[32].

Phases formed under hydrogen deficit. The lowest hydride, LaH_3, has been well studied at ambient and at moderate pressure. LaH_3 is an insulator and exhibits a pronounced Raman spectrum[28]. In our studies, we found that at $P > 100$ GPa, LaH_3 behaves as a poor metal or a semimetal, and it does not exhibit superconductivity upon cooling to ~5 K under pressures of at least 157 GPa.

Within the DAC, the lanthanum sample readily reacts with the surrounding hydrogen to form LaH_3, according to the Raman spectrum. This happens at $P \approx 10$ GPa at room temperature without any heat treatment. From the analysis of the X-ray powder diffraction patterns (Extended Data Fig. 1) at the high pressure of 152 GPa, we determined the crystal structure of sample 9 to be $Fm\bar{3}m$ with the refined lattice parameter $a = 4.3646(5)$ Å ($V = 83.14(3)$ Å^3, per formula unit $V = 20.78(3)$ Å^3). The LaH_3 stoichiometry for the sample was confirmed from the volume occupied by three H atoms—that is ~5.7 Å^3—which was obtained after the extraction of the volume of the La atoms ($V_{La} = 15.1$ Å^3; calculated using the equation of states for La from ref. [22]) from the volume per formula unit V. The stoichiometry of the compound cannot be higher than 1:3 (for example, LaH_4) because the volume of a hydrogen atom, V_H, is around 2 Å^3 according to extensive studies of hydrides under high pressures[33]. Lower stoichiometry (for example, LaH_2) is also impossible according to ref. [34], because this compound is not stable at pressures above 11 GPa and separates into LaH_3 and LaH_x, where x is 0.25 or 0.6–0.7. Thus, the only stoichiometry that can correspond to the cubic phase found experimentally is LaH_3. From the LaH_3 stoichiometry we can accurately determine the volume occupied by one hydrogen atom, which is approximately 1.9 Å^3 at 150 GPa. This estimation is valid even for higher pressures, as the unit-cell parameter $a = 4.313(2)$ Å refined for the fcc LaH_3 phase found in sample 10 at 178 GPa gave the same V_H of around 1.9 Å^3. The obtained 1.9 Å^3 volume occupied by one hydrogen atom at 150 GPa in LaH_3 provides a point of reference for estimating the stoichiometry of higher hydrides (and deuterides) as described in the main text.

We found superconductivity in the samples with an apparent hydrogen deficiency, but with lower T_c values. In particular, in the unheated mixture of La and H_2 pressurized up to 178 GPa (sample 10), we observed a pronounced and reproducible superconducting step at $T_c \approx 70$ K (Extended Data Fig. 2). The shift in T_c to a lower temperature (~49 K) upon the application of an external magnetic field (5 T) further verifies the superconducting nature of this transition. The sample absorbed the rest of the hydrogen after laser heating: its volume increased, and it transformed into a new superconducting phase with $T_c \approx 112$ K (Extended Data Fig. 2). This suggests that increasing the hydrogen content (stoichiometry) would lead to an increase in T_c. This superconductivity was reproduced in another sample (sample 9) synthesized at 152 GPa, with almost the same value of T_c (~108 K). Note that T_c increases with pressure for this phase. X-ray diffraction patterns of the laser-heated samples with T_c values of around 110 K and 70 K were found to be very complicated to analyse, perhaps because these samples consist of a mixture of phases (Extended Data Fig. 1). According to theoretical predictions, the following stable metallic compounds could exist at $P \approx 150$ GPa: LaH_4, LaH_6 and LaH_8 (ref. [5]), or only LaH_6 (ref. [3]). The calculated T_c values are 5–10 K at 300 GPa, 150–160 K at 100 GPa and 114–150 K at 300 GPa[5], for LaH_4, LaH_6 and LaH_8, respectively. The experimentally observed phase with $T_c \approx 110$ K can probably be assigned to either LaH_6 or LaH_8.

Phases formed under an excess of hydrogen. Superconductivity at a much higher T_c (215 K) was found in sample 12; this sample was surrounded by a larger amount of hydrogen that seems to have been absorbed in the synthesis procedure (Extended Data Fig. 3), as described in detail in ref. [24]. This phase apparently competes with the phase exhibiting T_c at 250 K, as it can be synthesized under the same pressures following the aforementioned laser-treatment procedure.

Isotope effect. A substitution of isotopes—that is, changing the mass of the atoms in a crystal—leads to a change in the phonon spectrum and, consequently, in the T_c; this is known as the isotope effect. Typically, it is assumed that the substitution does not alter the crystalline lattice as the Coulomb forces do not change. However hydrogen and deuterium are the lightest atoms and zero-point energy and anharmonic effects can influence the stability of the crystals. The effect of the difference in the hydrogen and deuterium energy can be noticeable, especially in cases where competitive structures are close in energy. A different phase sequence in deuterides and hydrides is a rare phenomenon. It was reported previously in the V-H/V-D system[35], where the large difference in zero-point energies for H and D atoms results in the occupation of different interstitials for these two isotopes and consequently different crystal structures.

We found a considerable difference between the La-H and La-D systems. Whereas the fcc-LaH_{10} phase dominates in the La-H system (samples 2 and 3), a phase with the tetragonally distorted fcc lattice *P4/nmm* (Fig. 3c) was found in most of the deuterides (samples 8, 15 and 16). We estimated the composition of this phase as LaD_{11} from the consideration of the lattice volume. We associate the 140–168 K superconducting phase in samples 8 and 15 with the dominant *P4/nmm* LaD_{11} structure (Extended Data Fig. 5). In these samples the LaD_{11} phase is accompanied by the hcp phase, which has a nearly ideal *c*/*a* ratio of around 1.63 (where *c* and *a* are the lengths of the respective sides of the unit cell), and a lattice volume close to that of the fcc-LaD_{10}. Hereafter this phase is denoted hcp-I LaD_{10}. We did not obtain this phase in a single phase state; however, if this phase is superconducting, its T_c is not higher than that of the *P4/nmm* LaD_{11} phase (140–168 K).

In other samples, the *P4/nmm* LaD_{11} phase (sample 16 and 17) is accompanied by another hexagonal phase, hcp-II, with a distorted *c*/*a* ratio of approximately 1.48 and a lattice volume smaller than that of the hcp-I LaD_{10} by around 1 $Å^3$, which could indicate a smaller hydrogen content in the hcp-II lattice (LaD_{10-x}, where $x \approx 0.25$). The nearly pure hcp-II phase (sample 14) exhibits no superconductivity at temperatures greater than 113 K (sample 14), which limits the potential superconductivity of this phase.

The fcc-LaD_{10} phase was found in samples 17 and 18. Sample 17 consists of a mixture with two hcp phases of LaD_{10} and another unidentified transparent impurity (Extended Data Fig. 6). Because the T_c of the hcp-I LaD_{10} phase is lower than 168 K, as discussed above, the T_c at around180 K can be attributed to the fcc-LaD_{10} phase. Further evidence is obtained by laser heating the fcc-LaD_{10} (as discussed above and in Extended Data Fig. 6). Sample 18, with the highest T_c (around 180 K) in the La-D system, contains a mixture of hcp-II LaD_{10}, fcc-LaD_{10} and some unidentified impurity (Extended Data Fig. 7).

In the La-H system, the highest T_c (around 250 K) was clearly attributed to the fcc-LaH_{10} phase, as it is the dominant phase in samples 2 and 3 (Fig. 3). Nevertheless, it is also accompanied by impurities of hcp-I and hcp-II phases with LaH_{10} stoichiometry—the same phases as those found in the La-D system. The hcp-I phase was found in sample 3 together with the fcc phase, and the hcp-II phase was found together with the fcc phase in sample 2 (with only traces of hcp-I). Both samples exhibit the same superconductive transition, with $T_c \approx 250$ K, despite the fact that the samples contain different impurity hexagonal phases; this indicates that superconductivity at $T_c \approx 250$ K originates from the fcc phase. In particular, traces of the hcp-I phase (~10%) are distributed heterogeneously in sample 2 and cannot be responsible for the abrupt superconductive transition to zero resistance (Fig. 1).

In contrast to the La-D system, we did not find the *P4/nmm* phase in La-H. However, we found a phase with a simple cubic lattice of LaH_{12} stoichiometry, which is absent in the deuterides. This semitransparent sample is insulating (sample 21). The sc-LaH_{12} compound was synthesized experimentally as an almost pure phase by heating LaH_3, rather than La, in hydrogen.

Notably, under H(D) deficiency in the pressure range of interest, LaH_3 and LaD_3 also have different crystal structures: *fcc* (samples 9 and 10) and *Cmcm* (sample 20), respectively. The latter has been predicted previously for LaH_3 in ref. [3]. The superconducting properties of these phases are very different: *Cmcm* LaD_3 (sample 20) has a T_c of around 68 K, whereas LaH_3, when synthesized separately and compressed in a DAC in an inert medium, did not exhibit superconductivity at temperatures as low as 5 K.

Data availability

The authors declare that the data supporting the findings of this study are available within the paper and its supplementary information files.

28. Meng, H., Kuzovnikov, M. A. & Tkacz, M. Phase stability of some rare earth trihydrides under high pressure. *Int. J. Hydrogen Energy* **42**, 29344–29349 (2017).
29. Eremets, M. I. & Troyan, I. A. Conductive dense hydrogen. *Nat. Mater.* **10**, 927–931 (2011).
30. Eremets, M. I. Megabar high-pressure cells for Raman measurements. *J. Raman Spectrosc.* **34**, 515–518 (2003).
31. Prescher, C. & Prakapenka, V. B. DIOPTAS: a program for reduction of two-dimensional X-ray diffraction data and data exploration. *High Press. Res.* **35**, 223–230 (2015).
32. Toby, B. H. EXPGUI, a graphical user interface for GSAS. *J. Appl. Crystallogr.* **34**, 210–213 (2001).
33. Fukai, Y. *The Metal-Hydrogen System* 2nd edn (Springer-Verlag, Berlin Heidelberg, 2005).
34. Machida, A., Watanuki, T., Kawana, D. & Aoki, K. Phase separation of lanthanum hydride under high pressure. *Phys. Rev. B* **83**, 054103 (2011).
35. Schober, T. & Pesch, W. The systems vanadium-hydrogen and vanadium-deuterium. *Z. Phys. Chem.* **114**, 21–28 (1979).

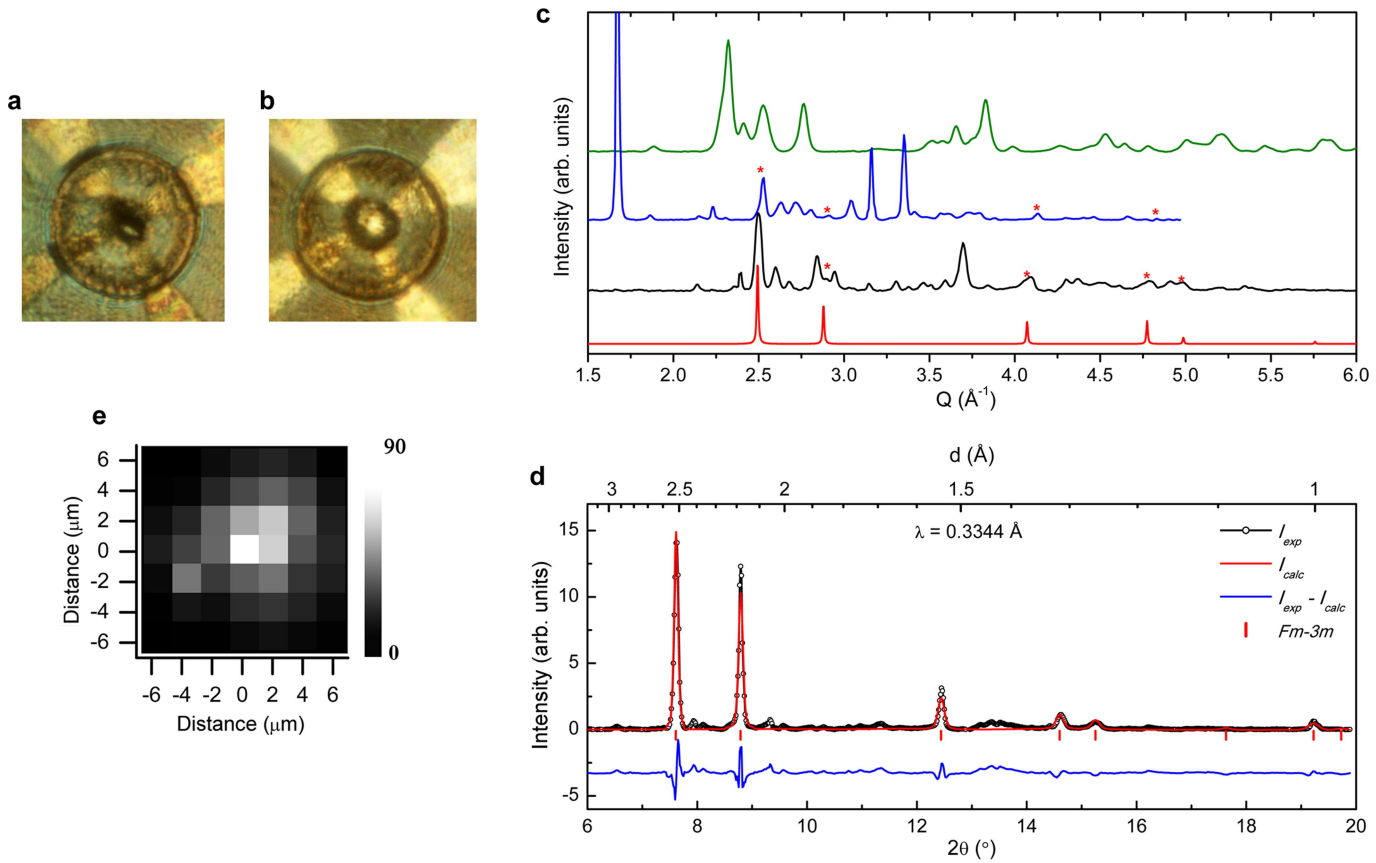

Extended Data Fig. 1 | Characterization of samples synthesized from a mixture of La + H_2 (in deficiency) at 150–180 GPa that exhibit superconductivity at around 70 K and around 110 K. a, **b**, Photographs of sample 9 exhibiting superconductivity with $T_c \approx 108$ K after laser heating. Photos are taken in the combined transmitting–reflecting illumination before (**a**) and after (**b**) laser heating at around 1,000 K at 152 GPa. After thermal treatment, the size of the sample increased considerably and it started to reflect the incident light. **c**, Typical integrated X-ray powder patterns for different samples synthesized from lanthanum heated in H_2 (in deficiency). We were unable to index the patterns from a complicated mixture of different phases. The black plot corresponds to sample 9 synthesized at 152 GPa with $T_c \approx 108$ K. The blue and olive plots correspond to samples 10 and 11 synthesized at 178 GPa ($T_c \approx 112$ K) and 150 GPa ($T_c \approx 70$ K), respectively. The red plot and red stars indicate the $Fm\bar{3}m$ phase of LaH_3 (two of the samples also contain some LaH_3 phase). **d**, The integrated X-ray powder pattern of sample 10 shown in b measured in the centre of the sample. It indicates an almost pure $Fm\bar{3}m$ phase of LaH_3. Black, red and blue plots correspond to experimental data, fitted data, and the difference between experimental and fitted data, respectively. **e**, The distribution of the fcc phase of LaH_3 in the heated sample 10, shown in **b**, obtained from mapping the sample with an X-ray focused beam. The brightest part in the centre corresponds to the powder pattern presented in **d**.

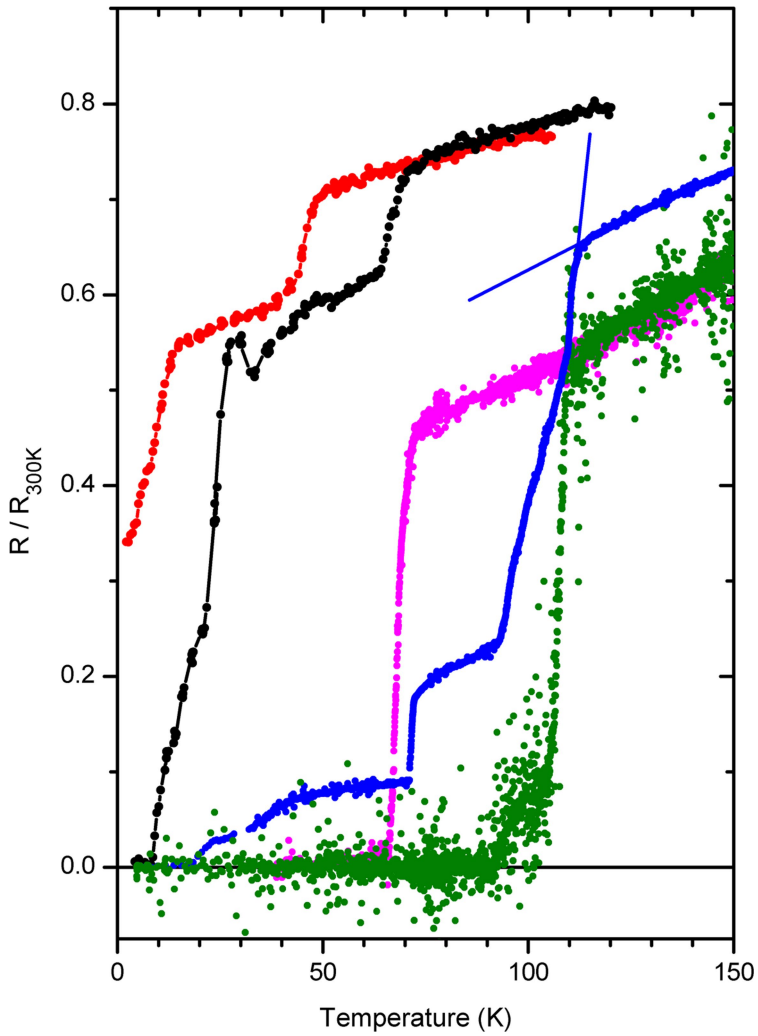

Extended Data Fig. 2 | Superconductive transitions occurring in different samples prepared from a mixture of La + H_2, when H_2 is taken in deficiency. Resistance was normalized to the value at 300 K for each sample. The unheated sample 10 at 178 GPa (black plot) shows the onset of the superconducting transition at around 70 K, which shifts with a magnetic field of 5 T to about 49 K (red plot). The same superconducting phase ($T_c \approx 70$ K; magenta plot) was found in another sample (sample 11) prepared at 150 GPa by laser heating of the La + H_2 mixture (in a large deficiency of H_2). After subsequent gradual laser heating of the first sample (black plot) up to about 1,500 K, the sample absorbed the rest of the hydrogen, its volume increased, and a new superconductive transition appeared at around 112 K (blue plot). After several heating cycles, only one sharp transition at 112 K remained (green plot). The T_c was determined from the onset of superconductivity, at the intersection of the temperature dependence of resistance in the normal and superconducting states (blue lines in the blue plot).

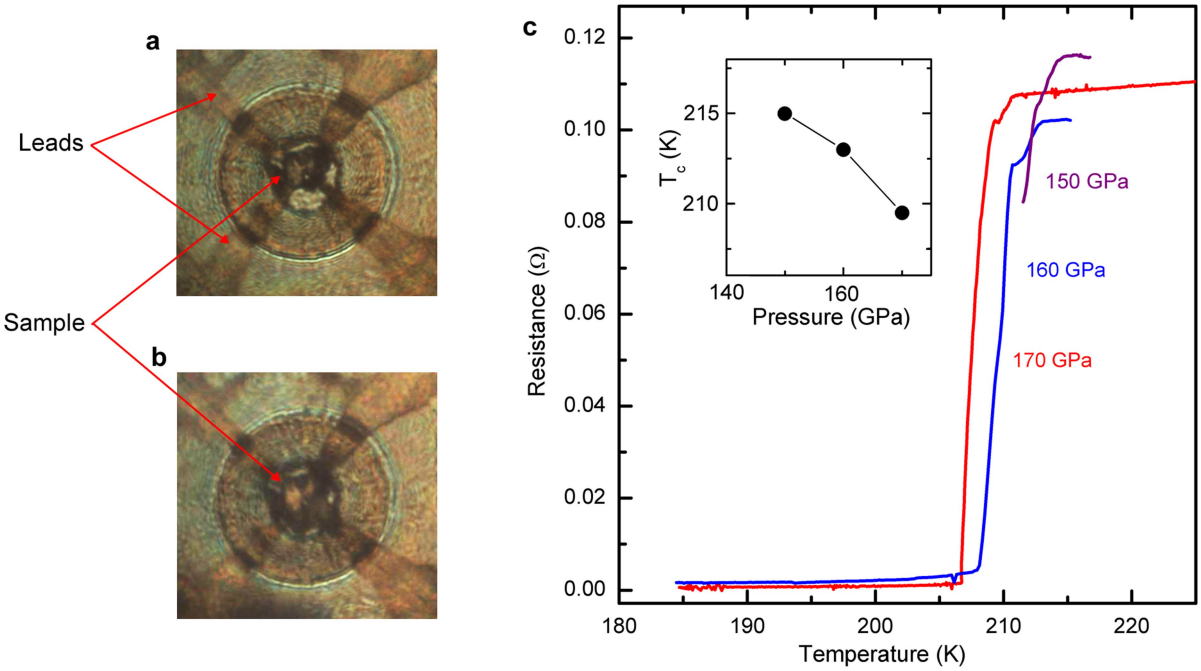

Extended Data Fig. 3 | Superconductivity in sample 12 synthesized at around 160 GPa from a mixture of lanthanum and an excess of H_2. **a**, **b**, View of the sample inside the diamond anvil cell with the attached four electrodes at transmission illumination before (**a**) and after (**b**) laser heating. As a result of heating, the sample increased considerably in volume and nearly filled the whole sample space, but was still surrounded by hydrogen. **c**, Superconducting steps shown by the temperature dependence of the resistance at different pressures. The pressure dependence of the onset of superconductivity is shown in the inset: T_c shifts to higher temperatures as the pressure is decreased.

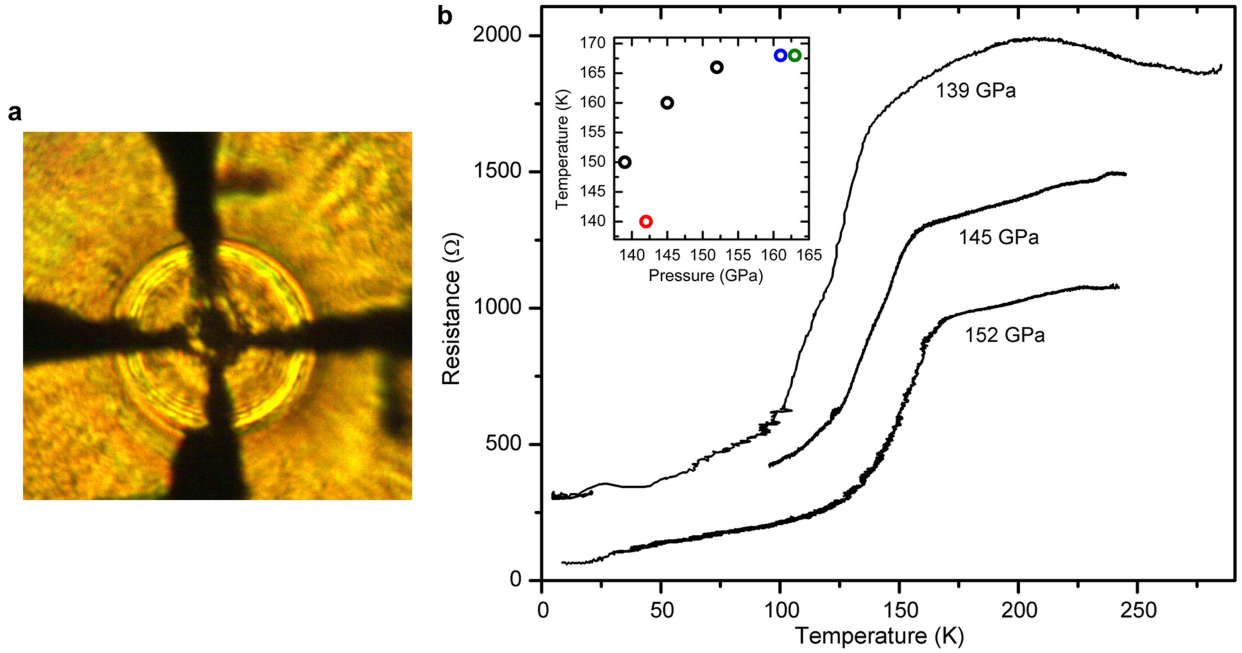

Extended Data Fig. 4 | Lanthanum samples heated by a laser in an excess of deuterium. a, Photograph of the heated LaD_{11} sample (13) at 139 GPa, taken in transmission illumination mode. **b**, Superconducting transitions at different pressures (the pressure was determined from the D_2 vibron scale[29]). The inset shows the pressure dependence of T_c measured for different samples (red, black, green and blue points correspond to samples 8, 13, 15 and 16, respectively). The refined crystal structure for red, blue and green points corresponds to the tetragonal *P4/nmm* lattice and LaD_{11} stoichiometry.

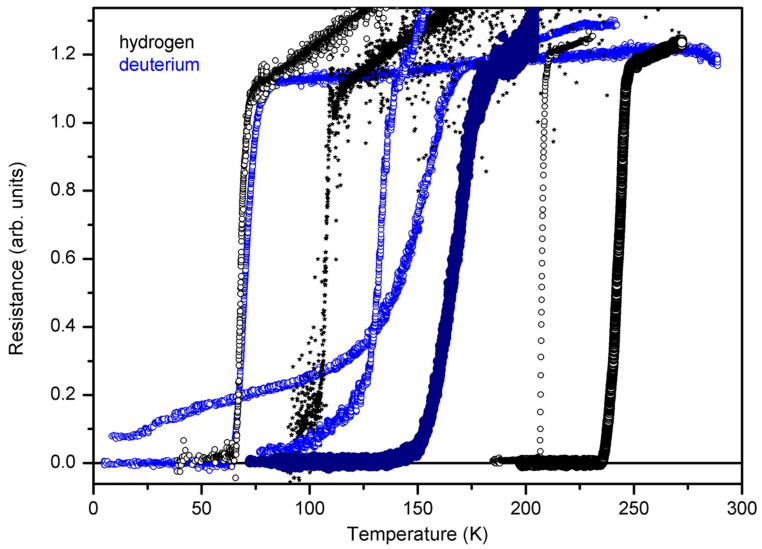

Extended Data Fig. 5 | Superconducting transitions in hydrides synthesized from lanthanum in hydrogen and deuterium atmospheres. Lanthanum hydrides: $T_c \approx 250$ K (sample 1), $T_c \approx 215$ K (sample 12), $T_c \approx 110$ K (sample 10), $T_c \approx 70$ K (sample 11); lanthanum deuterides: $T_c \approx 180$ K (sample 17), $T_c \approx 165$ K (sample 13), $T_c \approx 140$ K (sample 8) and $T_c \approx 80$ K (sample 14). The thick curves show the $R(T)$ dependences of the samples with fcc-LaH_{10} and fcc-LaD_{10} phases.

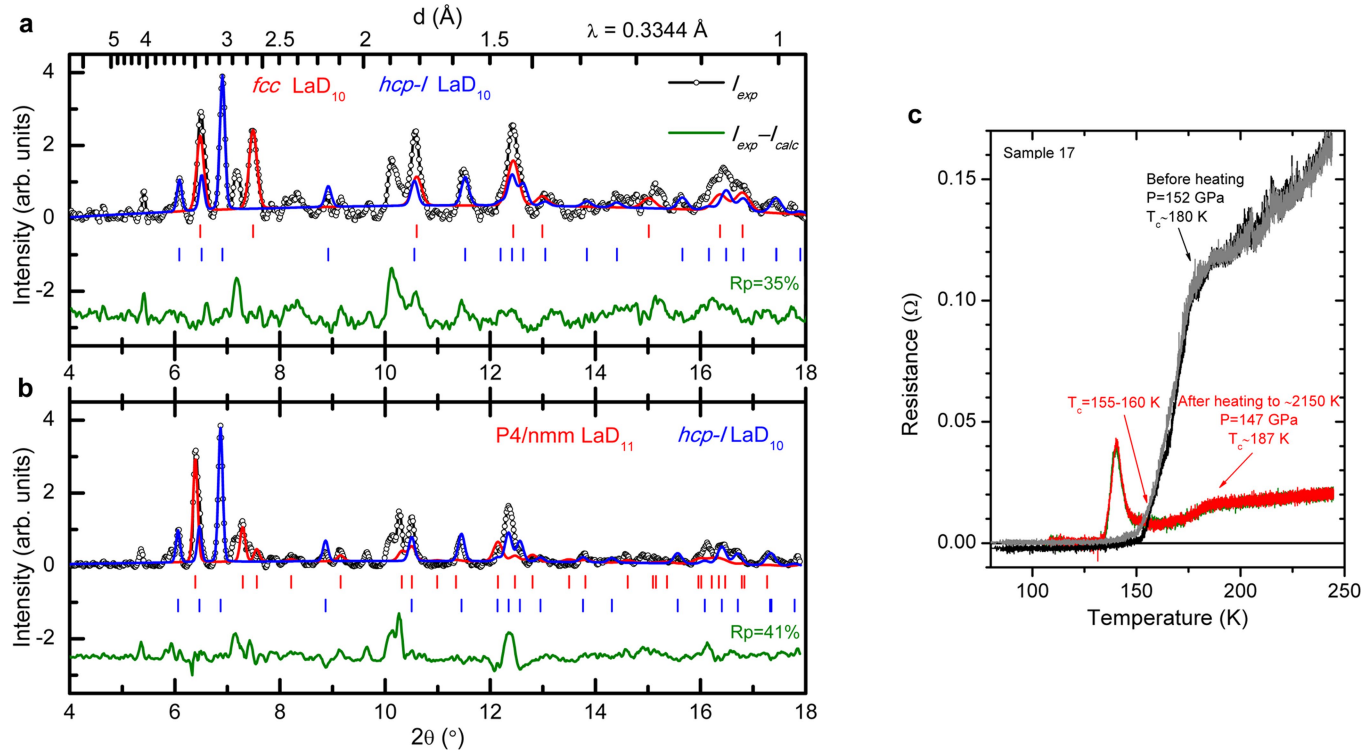

Extended Data Fig. 6 | Superconductivity in lanthanum deuteride with the fcc-LaD_{10} phase. a, The X-ray diffraction pattern of sample 17 before laser heating contains fcc-LaD_{10} as well as hcp-I and hcp-II LaH_{10} phases, and an unidentified transparent phase. The sample was synthesized at around 120 GPa by heating a piece of lanthanum in a deuterium atmosphere. The temperature dependence of resistance measured at 152 GPa reveals a superconducting transition with $T_c \approx 180$ K. **b**, As a result of successive laser heating to 2,150 K, a considerable amount of the fcc-LaD_{10} phase transformed into the *P4/nmm* LaD_{11} phase, while diffraction patterns from the impurities hcp-I, hcp-II and the unidentified transparent phases remained almost unchanged. **c**, In accordance with the structural change, a new peak on the $R(T)$ graph appeared at around 140 K. In fact, the shape of the $R(T)$ plot indicates a superconducting transition, as is observed in granular disordered systems (see, for instance, ref. [25]). In this case, the onset of superconductivity should be taken at a temperature when the peak starts to develop—that is, at 155–160 K, as indicated by the arrow. The subtle step at around 187 K on the red curve after laser heating relates to the remains of the fcc-LaD_{10} phase.

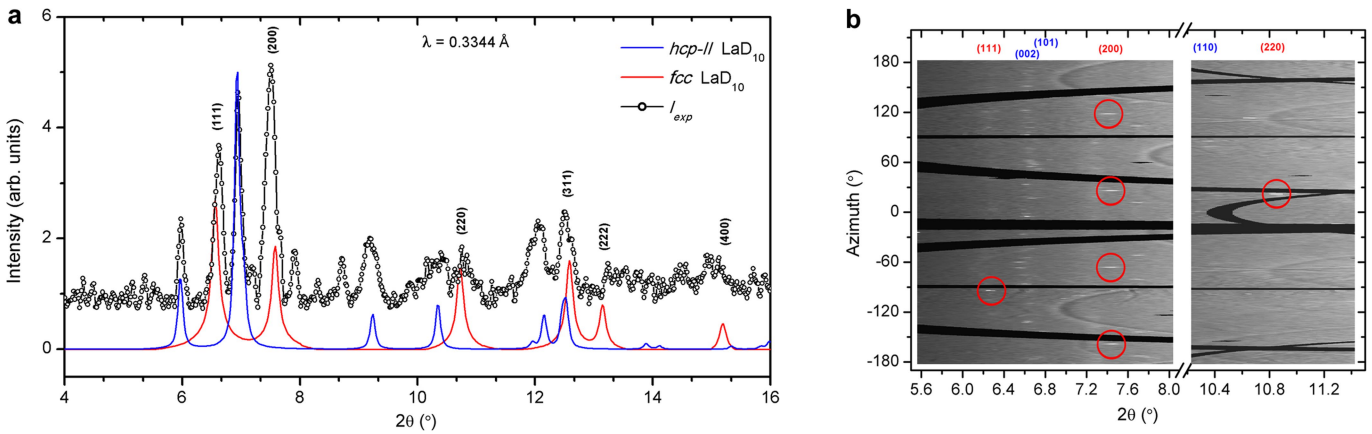

Extended Data Fig. 7 | X-ray powder diffraction analysis for sample 18 exhibiting a high T_c of approximately 180 K. a, Typical integrated X-ray powder diffraction pattern for sample 18 (black curve). The experimental powder pattern is obviously complex; nevertheless, most reflections can be indexed as corresponding to two phases: fcc-LaD_{10} (red pattern) and hcp-II LaD_{10} (blue pattern). **b**, The reflections from the fcc-LaD_{10} phase are represented as separate spots, indicated by the red circles in the cake representation of the X-ray powder diffraction pattern.